Proceedings of the ASME 2017 Dynamic Systems and Control Conference
DSCC2017
October 11-13, 2017, Tysons, Virginia, USA

DSCC2017-5208

DIRECT TAIL ACTUATION VS. INTERNAL ROTOR PROPULSION IN AQUATIC ROBOTS

Beau Pollard
Department of Mechanical Engineering
Clemson University
Clemson, South Carolina 29631
Email: bpollar@g.clemson.edu

Tyler Berkey
Department of Mechanical Engineering
Clemson University
Clemson, South Carolina 29631
Email: tberkey@g.clemson.edu

Phanindra Tallapragada*
Department of Mechanical Engineering
Clemson University
Clemson, South Carolina 29631
Email: ptallap@clemson.edu

ABSTRACT

It is common for scientists to look to nature for inspiration in developing robots. Many times biological creatures outperform even the best man made robots. We will be focusing on aquatic locomotion of robots inspired by the locomotion of fish. There are two different means of propulsion of the robots tested in this paper. One model of the robot is propelled only through the oscillations of an internal momentum wheel, while the other is propelled by the direct actuation of a tail structure. Both of these models achieve net propulsion through vortex shedding past their trailing edge, and two of the robots locomotion is also aided by the change in shape from either a passive or active tail. Tests were conducted to highlight the locomotion performance differences of the two different means of locomotion.

1 INTRODUCTION

In the past decade, there has been a significant amount of research dedicated to developing aquatic robots whose locomotion mimics or is inspired by the locomotion of natural swimmers [1–12]. Researchers hope that by harnessing the propulsive properties of natural swimmers, their robots will be able to mimic some of the characteristics of fish. Different species of fish demonstrate locomotion characteristics such as efficient swimming, high degree of maneuverability and the potential for swift speeds. The common design feature of bioinspired swimming robots is that they propel themselves by producing changes in the shape of their body. This results in a change in the inertia tensor of the body as well as producing vorticity at the sharp edges of the tails or fins that produce periodic propulsive force.

Different species of natural swimmers possess quite different locomotion characteristics, and so there are a number of different types of bio-inspired robots. Anguilliform swimmers, such as eels, achieve locomotion thought large amplitude undulations of their entire body. Robots mimicking anguilliforms have a high degree of freedom meaning their bodies are controlled by a large number of servos [13–16]. The high degree of freedom of these robots allow for high maneuverability but their swimming speeds are limited. Additionally researchers have developed robots inspired by carangiforms, such as tuna, and subcarangiforms such as trout, whose locomotion is provided by the undulations of a tail segment(s) [3, 4, 17–21]. These types of robots typically have fewer degrees of freedom then anguilliform robots, making them less maneuverable. The undulations of the tail produce an enhanced propulsive force, meaning that these types of robots are typically capable of rapid speeds [22]. The robots tested throughout this paper are inspired by carangi-

*Address all correspondence to this author.

form fish.

Directly actuating tail segments is not the only way to acheive net locomotion in a bio-inspired robot. The authors have shown in previous work [23–27] that a solid symmetric hydrofoil can swim through the oscillations of an internal momentum wheel. Since the robots are solid bodies, there are no physical shape changes to provide propulsion, the propulsion of the robot is made possible by the shedding of vortices past the trailing edge of the robot. This model while inspired by the mechanics of swimming of fish avoids the exact mimicking of the shape changes of the body of a fish.

In this paper we will present experimental results comparing the maneuverability and speed of a robot propelled by an internal rotor and a robot with a directly actuated tail. The geometries and weights of the robots throughout the tests are all similar. The internally propelled robot tested in this paper has two different configurations. During the straight line speed tests, the directly actuated robot's speed will be compared to a solid body robot. The servo motors used on the different robots have the same characteristics, to maintain a similarity in all design aspects of the different models. For the turning tests, a robot with the same main body cross section is tested, but there is a passive tail added to the model. The passive tail aids in maneuverability, and is similar in dimensions to the tail of the directly actuated tail on the externally driven robot.

The paper is organized as follows, in section 2 we describe in detail the different robots tested in this paper. In section 3, the experiments are reviewed and the inputs of the motors for the respective tests are stated. In section 4 we review the experimental results of the different tests.

2 MODELS

The models tested are shown in Fig. 1. Figure 1-(a) shows A robot with a directly actuated tail, Fig. 1-(b) shows the robot with a passive tail and propelled by an internal rotor, and Fig. 1-(c) is the solid body robot propelled by an internal momentum wheel. Throughout the paper the robots will be referred to as robots A, B and C respectively. The robots are of similar dimensions and weights. Robot A weighs 1200 grams, robot B weighs 1150 grams and robot C weighs 1100 grams. Their main bodies were designed to have the horizontal cross section of a NACA 0030 symmetric Joukowski foil. The tail sections of robots A and B make up approximately one third of the length of the robots and are of similar cross section dimensions as the back third of robot C. The momentum wheel of the internally driven robot makes up a significant part of the mass (40%) so the directly actuated robot was weighted with bolts and a smaller internal rotor to make the total weight similar to the weights of the internally propelled robots.

Robot B has a tail segment, but this tail is passive, i.e. that the tail is not directly actuated by a motor but only by the coupled fluid body interaction. Robot C possesses no appendages so there is no body shape change to contribute to its locomotion, its propulsion depends only on the shedding of vortices.

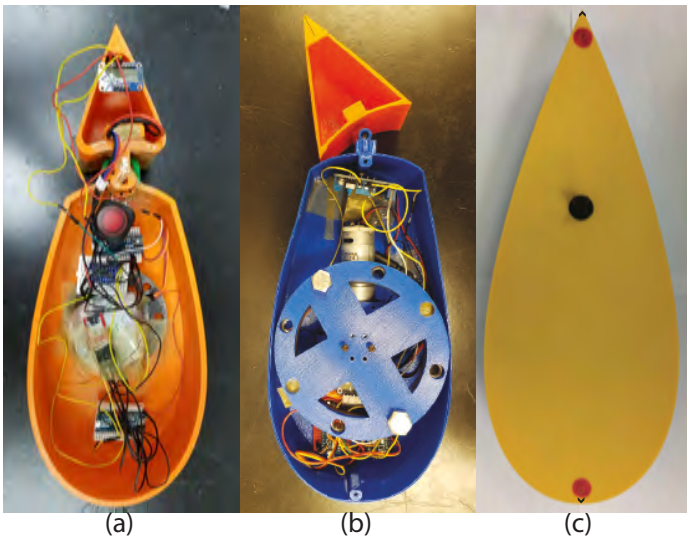

FIGURE 1: (a) ROBOT WITH A DIRECTLY ACTUATED TAIL, (b) ROBOT PROPELLED BT AN INTERNAL MOMENTUM WHEEL POSSESSING A PASSIVE TAIL, (c) SOLID BODY ROBOT DRIVEN BY AN INTERNAL MOMENTUM WHEEL

Figure 2 shows a 2D representation of the robots. The solid blue line in Fig. 2 represents the entire body of robot C and the front two thirds of the main bodies of robots A and B. The dashed red line in Fig. 2 represents the tail segments of robots A and B. The X and Y axes coordinates represent the inertial coordinates. During the tests, the X axis is aligned with the longitudinal axis of the test pool. X_b and Y_b are the body fixed axes of the robots; the X_b axis is created by drawing a line connecting the point that the tail is connected to the tip of the main body. The angular orientation of the robots main bodies is denoted by θ, which is the angle measured from the X axis to the X_b axis, and the angular orientation of the tail is denoted as β, which is the angle measured from the X axis to a line connecting the trailing edge

of the tail to the point where the tail connects with the main body.

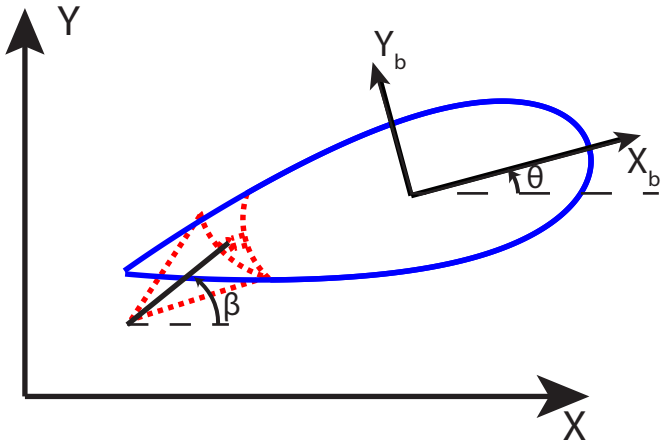

FIGURE 2: 2-D REPRESENTATION OF THE ROBOTS

3 EXPERIMENTS

The experiments conducted in this paper were designed to give a comparison of the robot propelled through the direct actuation of a tail to a robot of similar dimensions driven by an internal momentum wheel. The first tests compare the maneuverability of robots A and B. In this paper maneuverability is characterized as the turning radius, θ_r, and turning time, t_t. The turning radius θ_r is described as the displacement in the Y and X axis of the main body measured from the time that the robots turning phase starts until $\theta = 180^o$, and the turning time t_t is the time it takes for $\theta = 180^o$.

The turning phases of the robots were different due to their difference in means of propulsion. The robot with an actuated tail turned by flapping its tail between the maximum angle β_{max} and the minimum angle β_{min} slowly, and then rapidly back to β_{max}. After a short delay this process was repeated until the $\theta \approx 180^o$. The robot propelled by an internal rotor performed a turn by first applying a constant angular velocity $\omega_r = 825^o/s$ to the internal momentum wheel. The momentum wheel then slowed to a stop before beginning to rotate with a constant angular velocity again.

The second set of experiments were designed to compare the average straight line speed of robots A and C. The average speed is compared and not the true speed since the trajectories of the robots is sinusoidal with the heading angle showing small periodic variations. This is more pronounced in the motion of robot C. However the net displacement over many such time periods is nearly along a straight line. Since this paper is strictly a comparison of the different means of propulsion, we compare models with similar motors. We found that in order for robot B to achieve net propulsion it needed to have a low frequency, high amplitude sinusoidal input, which could not be provided by the limited range of rotation of the servo motor used in model A and C.

During these tests motors were given the following inputs

$$\omega(t) = \begin{cases} \omega_r & : nT < t \leq nT + \frac{T}{2} \\ -\omega_r & : nT + \frac{T}{2} < t \leq (n+1)T \end{cases} \quad (1)$$

where n is a non-negative integer and

$$T = \frac{4\phi_t}{\omega_r}.$$

In Eqn. 1, ω_r is the magnitude of the angular velocity of the tail segment and ϕ_t is the amplitude of the tail oscillations. In order to track the position of the robots, a grid with lateral and longitudinal lines every 10 cm was placed at the bottom of the pool. A camera mounted above the pool was used to capture videos during the tests. Using the videos with the grid lines, we were able to determine average velocities for the robots during the straight line tests as well as the turning radius during the turning tests. During all of the tests, the Z value remains the same, meaning we are only focused on planar motion of the robots.

4 RESULTS

The first test quantifies the maneuverability of the two robots. Figure 3 shows the angular orientation θ of the robots throughout their turning phases. In Fig. 3, the solid red line represents the heading angle, θ, of the robot propelled by an internal rotor, while the dashed blue line represents the heading angle of the directly actuated robot. The internally actuated robot had a turning time $t_t \approx 8.3s$, while the robot with a directly actuated tail had a turning time $t_t \approx 15.3s$. This shows that the internal rotor robot reached a turning angle of $\theta = 180^o$ approximately 45% sooner then the directly actuated robot.

Figure 4 shows the X and Y positions of the robots throughout their turning phases. The solid red line represents the po-

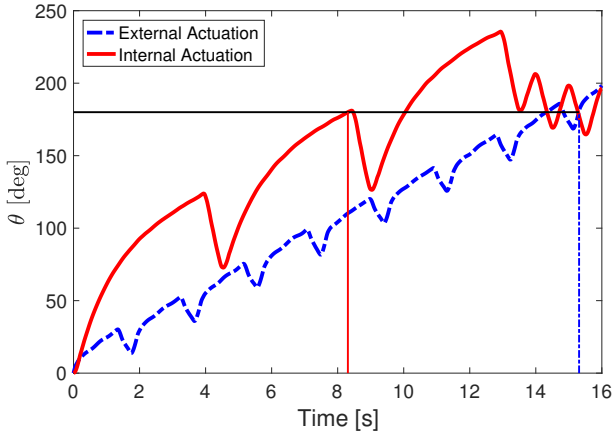

FIGURE 3: GYRO DATA FOR THE TWO ROBOTS DURING THEIR TURNING PHASES

sition of the internally actuated robot and the dashed blue line represents the directly actuated robot.

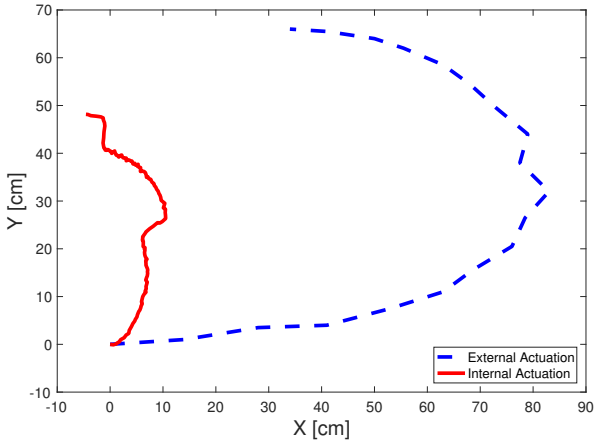

FIGURE 4: TURNING RADIUS θ_r OF THE TWO ROBOTS

The internally actuated robot had a turning radius $\theta_r \approx 49$ cm, while the externally actuated robot had a turning radius of $\theta_r \approx 65$ cm. This shows that the internally actuated robot had a turning radius approximately 25% smaller than the externally actuated robot. Additionally, the displacement required to allow the turn to be successful was larger for the externally actuated robot. For the internally actuated robot, a maximum displacement of approximately $15cm$ is required, while the externally actuated robot required a maximum displacement 5.6 times larger, at approximately 84 cm.

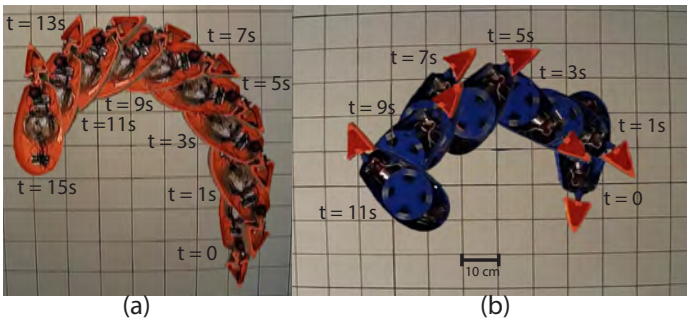

FIGURE 5: SNAPSHOTS OF THE ROBOTS PERFORMING TURNS

Figure 5 shows snapshots of the robots during their turns overlaid on an image of the pool. Figure 5 gives a physical representation of the total pose of the robots during their turning phases. From Figs. 3, 4 and 5 it is apparent that once the turning phases were started the robot propelled by an internal momentum wheel initially rotated significantly faster than the directly actuated robot. The reason for this is that the constant angular rotation of the internal momentum wheel produced a large change in the angular momentum of the body while providing very little change in the linear momentum. Robot A on the other hand had to rotate its tail in both directions, i.e. that its change in angular momentum was accompanied by a change in the bodies linear momentum. Once robot A's body achieved a $\theta \approx 50^o$ its angular acceleration diminished. It completed the next 130^o of the turn in approximately the same time as robot B completed. The initial faster turn rate of robot B, allowed it to have an overall faster turn time.

In the second tests, the average speeds over 10 cm segments were calculated for robots A and C; the results from this test are shown in Fig. 6.

The speeds were measured by looking at the individual frames of the videos taken during the tests and measuring how long it took for each robot to move from one grid line to the next. Robot A reached a top average speed of approximately 16 cm/s and robot C reached a top average speed of approximately

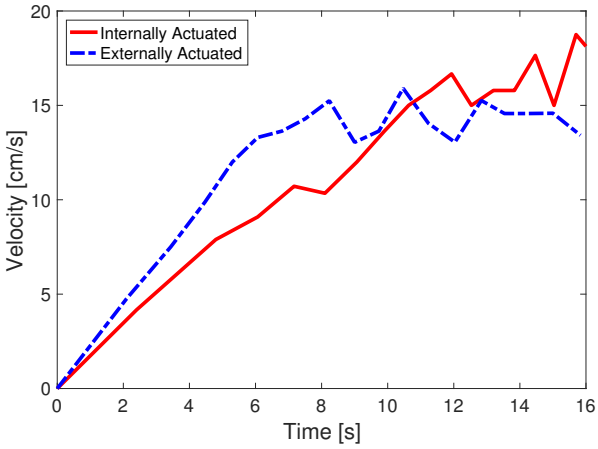

FIGURE 6: PLOT OF THE AVERAGE SPEEDS OF THE ROBOTS DURING ON AVERAGE STRAIGHT LINE MOTION

18 cm/s. In Fig. 6 it is apparent that robot A accelerated to its steady state speed quicker then robot C, but robot C's top speed was approximately 2 cm/s faster then robot A's. Robot C's speed never reached a stable steady state speed due to the limitations of pool length and also the large waves produced from the high frequency oscillations of the body in the water. With a longer and a wider pool, the robot C's top average speed could increase.

The robots were weighed and designed similarly to highlight the difference in performance of the two means of propulsion, but robot A is not limited by the same size constraints as robots B and C. Robots B and C are limited in the amount their size can be reduced because their internal momentum wheels take up a large amount of space and make up a significant portion of the robots weight. The relationship between rotor size/weight and body size doesn't scale linearly, so decreasing the body size and rotor size does not result in similar swimming characteristics. Robot A, on the other hand, is not limited by a large rotor, so its body size and weight could be significantly reduced easily, which would result in better locomotion performance. We removed the additional weight from robot A and it was able to reach a top average speed of 16.6 cm/s. While this value is higher than the weighted down version, it is still not as fast as robot C, but if robot A's body was reduced in dimension it would likely be able to reach significantly faster speeds.

5 CONCLUSION

Through a series of three tests, the performance of all three robots has been analyzed. The internal rotor design provides a faster turn time, a smaller turning radius, as well as a faster maximum straight line speed for robots of similar dimensions. This does not necessarily mean that robots with internal momentum wheels are more efficient or maneuverable swimmers than ones with actuated tails. Utilizing a directly actuated tail allows for a significant reduction in body size and weight, which could lead to significantly better locomotion performance. It is however apparent that the ability of the rotor to significantly change the angular momentum of the robot without adding a large amount of linear momentum is beneficial for turning. Combining both direct actuation and internal actuation in the future may allow significant improvements to the performance of aquatic robots.

6 ACKNOWLEDGMENTS

This paper is based upon work supported by the National Science Foundation under grant number CMMI 1563315.

REFERENCES

[1] Triantafyllou, M. S., and Triantafyllou, G. S., 1993. "Propulsion through oscillating foils in nature and technology". *Journal of Fluids and Structures,* ***7***, pp. 205–224.

[2] Xiong, H., 2007. "Geometric mechanics, ideal hydrodynamics, and the locomotion of planar shape-changing aquatic vehicles". PhD thesis, University of Illinois at Urbana-Champaign.

[3] McGovern, S., Alici, G., Truong, V.-T., and Spinks, G., 2009. "Finding nemo (novel electromaterial muscle oscillator): a polypyrrole powered robotic fish with real-time wireless speed and directional control .". *Smart Materials and Structures.,* ***18***(9), p. 095009.

[4] Epps, B. P., P. Valdivia Alvarado, K. Y.-T., and Techet, A. H., 2009. "Swimming performance of a biomimetic compliant fish-like robot". *Experiments in Fluids,* ***47***, pp. 927–939.

[5] Chen, Z., Shatara, S., and Tan, X., 2010. "Modeling of biomimetic robotic fish propelled by an ionic polymermetal composite caudal fin.". *IEEE/ASME TRANSACTIONS ON MECHATRONICS,* ***15***(3), pp. 448–459.

[6] Rossi, C., Colorado, J., Coral, W., and Barrientos, A., 2011. "Bending continuous structures with smas: a novel robotic fish design". *Bioinspiration and Biomimetics,* ***6***, p. 045005.

[7] Rufo, M., and Smithers, M., 2011. "Ghostswimmer auv: Applying biomimetics to underwater robotics for achievement of tactical relevance.". *Marine Technology Society Journal,* ***45***(4), pp. 24–30.

[8] Kopman, V., and Porfiri, M., 2013. "Design, modeling, and characterization of a miniature robotic fish for research and education in biomimetics and bioinspiration.". *IEEE/ASME Transactions on Mechatronics,* ***18***(2), pp. 471–483.

[9] Shao, J., Wang, L., and Yu, J., 2008. "Development of an artificial fish-like robot and its application in cooperative transportation". *Control Engineering Practice,* ***16***(5), pp. 569–584.

[10] Papadopoulos, E., Apostolopoulos, E., and Tsigkourakos, P., 2009. "Design, control, and experimental performance of a teleoperated robotic fish". In 17th Mediterranean Conference on Control & Automation.

[11] Alvarado, P. V., and Youcef-Toumi, K., 2006. "Design of machines with compliant bodies for biomimetic locomotion in liquid environments". *ASME Journal of Dynamics Systems Measurement and Control,* ***128***(3-13).

[12] Zhou, C., and Low, K. H., 2012. "Design and locomotion control of a biomimetic underwater vehicle with fin propulsion". *EEE/ASME Trans. Mechatronics*.

[13] Liljeback, P., 2011. "Modelling, development, and control of snake robots". PhD thesis.

[14] Wang, K., and Ma, S., 2010. "Kinematic analysis of snake-like robot using sliding joints". In Robotics and Biomimetics (ROBIO), 2010 IEEE International Conference on, IEEE, pp. 1484–1489.

[15] Yu, S., Ma, S., Li, B., and Wang, Y., 2009. "An amphibious snake-like robot: Design and motion experiments on ground and in water". In Information and Automation, 2009. ICIA'09. International Conference on, IEEE, pp. 500–505.

[16] Manfredi, L., Assaf, T., Mintchev, S., Marrazza, S., Capantini, L., Orofino, S., Ascari, L., Grillner, S., Wallén, P., Ekeberg, Ö., et al., 2013. "A bioinspired autonomous swimming robot as a tool for studying goal-directed locomotion". *Biological cybernetics,* ***107***(5), pp. 513–527.

[17] Kopman, V., Laut, J., Acquaviva, ., Rizzo, A., and Porfiri, M., 2014. "Dynamic modeling of a robotic fish propelled by a compliant tail.". *IEEE Journal of Oceanic Engineering*, pp. 1–13.

[18] Liao, B., Li, Z., and Du, R., 2014. "Robot fish with a novel biomimetic wire-driven flapping propulsor". *Advanced Robotics,* ***28***(5), pp. 339–349.

[19] Morgansen, K. A., Triplett, B. I., and Klein., D. J., 2007. "Geometric methods for modeling and control of free-swimming fin-actuated underwater vehicles.". *IEEE Transactions on Robotics*.

[20] Jr, L. H. L., Krenitsky, N. M., Roberts, S. F., Cirokawa, J., de Leeuw, J., and Porter., M. E., 2011. "Testing biomimetic structures in bioinspired robots: how vertebrae control the stiffness of the body and the behavior of fish-like swimmers.". *Integrative and Computational Biology,* ***51***(1), pp. 158–175.

[21] Salumäe, T., and Kruusmaa, M., 2013. "Flow-relative control of an underwater robot". In Proc. R. Soc. A, Vol. 469, The Royal Society, p. 20120671.

[22] Raj, A., and Thakur, A., 2016. "Fish-inspired robots: Design, sensing, actuation, and autonomya review of research". *Bioinspiration & biomimetics,* ***11***(3), p. 031001.

[23] Tallapragada, P., and Kelly, S. D., 2013. "Reduced-order modeling of propulsive vortex shedding from a free pitching hydrofoil with an internal rotor". In Proceedings of the 2013 American Control Conference.

[24] Tallapragada., P., and Kelly, S. D., 2015. "Self-propulsion of free solid bodies with internal rotors via localized singular vortex shedding in planar ideal fluids". *The European Physical Journal Special Topics*.

[25] Tallapragada, P., 2015. "A swimming robot with an internal rotor as a nonholonomic system". *Proceedings of the American Control Conference, 2015*.

[26] Pollard, B., and Tallapragada, P., 2017. "An aquatic robot propelled by an internal rotor". *IEEE Transactions on Mechatronics,* ***22***(2), pp. 931 – 939.

[27] Pollard, B., and Tallapragada, P., 2016. "Fish like robot demonstrates characteristics of a linear system". In Proceeding of the ASME 2016 Dynamic Systems and Control Conference.